Objective Assessment of Extratropical Weather Systems in Simulated Climates

MARK R. SINCLAIR

National Institute of Water and Atmospheric Research Ltd., Wellington, New Zealand

IAN G. WATTERSON

Division of Atmospheric Research, CSIRO, Melbourne, Victoria, Australia, and
Cooperative Research Centre for Southern Hemisphere Meteorology, Clayton, Victoria, Australia

(Manuscript received 3 March 1998, in final form 11 March 1999)

ABSTRACT

An automated weather system identification and tracking scheme is used to appraise the skill of the CSIRO9 GCM in replicating contemporary extratropical cyclone and anticyclone behavior, and to assess possible changes as a result of doubled CO_2. Cyclones are identified as centers of cyclonic vorticity rather than pressure minima, which can vanish if the background pressure gradient increases. Comparison with an observational dataset from ECMWF revealed that the GCM control simulation realistically reproduced the present-day storm track locations, but with slightly fewer and generally weaker systems overall. These errors are consistent with the coarser resolution of the GCM and its underestimation of the strength and baroclinicity of the polar vortex in both hemispheres.

Comparison between 1 and 2 $\times$ CO_2 GCM simulations revealed increases in both 500-hPa geopotential height and 1000–500-hPa thickness for doubled CO_2. As in other studies, these changes are largest near the poles, resulting in weaker westerlies and reduced tropospheric baroclinicity. Decreases of 10%–15% in both cyclone and anticyclone activity consistent with these circulation changes are found. However, there is some evidence of increased winter cyclone activity near the downstream end of the principal storm tracks. There is also a general reduction in the number and strength of intense storms, despite generally lower central pressures, which arise from global-scale decreases in sea level pressure in the doubled CO_2 atmosphere rather than from greater storm vigor. This underscores the need for GCM projections of midlatitude ''storminess'' to employ more realistic measures of storm activity and intensity.

1. Introduction

Assessing the skill of general circulation models (GCMs) is fundamental to their use in understanding present and future climate. Model limitations must be determined and taken into consideration when evaluating GCM simulations of climate variability and future climate change scenarios. We can have most confidence in predictions of climate change from those GCMs best able to replicate present-day conditions. Model validation is thus an integral component of any GCM climate study. Verification studies also provide insights that can aid interpretation of GCM results and facilitate model improvements.

Systematic model climate errors are generally diagnosed by examining a standard set of time-averaged model output fields over the globe and comparing against observations (Gates 1992). However, a growing number of GCM validation and climate studies are using synoptic weather system climatologies based on automated feature identification and tracking algorithms (Lambert 1988, 1995; Murray and Simmonds 1991b; König et al. 1993; Hodges 1994, 1996; Zhang and Wang 1997; Hudson and Hewitson 1997; Hudson 1997; Blender et al. 1997). Because synoptic systems involve complex interactions on a range of space and time scales, their climatologies provide a comprehensive and exacting means of assessing GCM results. Cyclones and anticyclones form in preferred regions where the mean structure of the atmosphere favors their growth, while the associated heat and momentum transports in turn help to maintain the time-averaged circulation. Weather system statistics thus yield qualitative insights into atmospheric motions ranging from the general circulation down to subgrid-scale processes like condensation and air–sea exchange that modulate their growth. Since midlatitude climate is largely determined by the regular passage of migratory cyclones and anticyclones, objective weather system climatologies are also being used to

Corresponding author address: Dr. Mark R. Sinclair, Embry-Riddle Aeronautical University, 3200 Willow Creek Rd., Prescott, AZ 86301.
E-mail: sinclam@pr.erau.edu

assess how ''storminess'' on the one hand, or the frequency of settled spells on the other, might change under climate change scenarios. For example, Zhang and Wang (1997) documented a decrease in baroclinic eddy activity under a greenhouse warming scenario simulated by the National Center for Atmospheric Research (NCAR) Community Climate Model. They attributed this decrease to a reduced meridional temperature gradient, reduced land–sea contrasts, and increased poleward transport of moisture. Lambert (1995) also found a drop in the global frequency of extratropical cyclones in response to doubled CO_2 as simulated by the Canadian Climate Centre GCM, but with an increase in the number of lows having central 1000-hPa heights lower than −100 m. Katzfey and McInnes (1996) found a reduction in the number of eastern Australian cutoff lows in a $2 \times CO_2$ simulation by the Commonwealth Scientific and Industrial Research Organisation nine-level GCM (CSIRO9 GCM). However, those cyclones remaining tended to be more intense as a result of the greater role played by latent heating. Simmonds and Wu (1993) and Murray and Simmonds (1995) also used an objective tracking scheme to investigate the response of cyclones to changes in sea ice extent.

Objective finding and tracking algorithms based on long series of gridded analyses of observational data have been successfully used to survey the present-day behavior of surface cyclones (Jones and Simmonds 1993; Sinclair 1994, 1995), anticyclones (Jones and Simmonds 1994; Sinclair 1996), and upper-air features (Bell and Bosart 1989; Lefevre and Neilsen-Gammon 1995; Dean and Bosart 1996). They have also been used to identify systematic cyclone handling errors in operational numerical models (Akyildiz 1985). Automated techniques can now produce results in good agreement with the time-honored manually produced climatologies provided the method of finding and counting features is consistent with that used in the manual study (Sinclair 1997). Clearly, manual identification and tracking of synoptic systems is not feasible for GCM runs spanning several decades. Automated procedures also avoid the subjective choices made in manual studies and yield repeatable results.

Bandpass-filtered geopotential variance statistics are widely used as a proxy for storm track activity in studies of the general circulation (Blackmon et al. 1984; Wallace et al. 1988; Lau 1988) and for assessing storminess in GCMs (Hall et al. 1994; Carnell et al. 1996; Zhang and Wang 1997). This variance, which typically arises from the succession of mobile troughs and ridges within the westerlies, has the advantage of being directly linked to the eddy fluxes that help to maintain the mean flow (e.g., Trenberth 1991). Unfortunately, eddy statistics make no distinction between positive and negative fluctuations, making it difficult to treat cyclones and anticyclones separately. It is also difficult to isolate individual intense events from eddy statistics, which may not even contribute variance if they are slow moving. Furthermore, prolonged settled spells that are also an important component of midlatitude climate, are typically associated with persistent, slow-moving high pressure regions that contribute little to storm track variance.

In this paper, we use an objective feature identification and tracking algorithm to first assess the realism of simulations of the present climate and then to predict possible changes in weather system behavior resulting from enhanced greenhouse warming, as simulated by the CSIRO9 GCM (Watterson et al. 1995). Global extratropical cyclone and anticyclone statistics are constructed from a 30-yr series of 8-h 1000-hPa geopotential from a control ($1 \times CO_2$) simulation of the GCM. Observed data used for model validation are from twice-daily analyses from the European Centre for Medium-Range Weather Forecasts (ECMWF) during 1980–95 (Southern Hemisphere) and 1980–86 (Northern Hemisphere).

In the second part of this study, comparisons of statistics from 1 and $2 \times CO_2$ 30-yr runs of the CSIRO9 GCM are used to assess possible impacts of greenhouse warming on the frequency, location, and intensity of extratropical weather systems as simulated by the GCM. The procedures used in this study avoid sources of possible bias and incorporate a more realistic measure of storm intensity than past studies. These are important considerations when addressing the important question of how storminess might change under a warmer climate. The methodology outlined here can be readily applied to assessing climate change impacts from other GCMs.

In the following section, we briefly describe the CSIRO9 GCM while section 3 outlines the objective weather system finding and tracking procedures. Section 4 compares results from the GCM control simulation with those from ECMWF, while in section 5, statistics from 1 and $2 \times CO_2$ runs of the model are compared. Results are discussed in section 6.

2. The CSIRO9 GCM

The GCM used in the study is the Mark 2 version of the CSIRO9 (Gordon and O'Farrell 1997). The model uses the spectral method of representing the primitive equations, with a horizontal resolution truncated at R21, a transform grid of 56 latitudes and 64 longitudes, and nine sigma levels in the vertical. It includes a semi-Lagrangian moisture transport scheme, but otherwise rather standard parameterizations of convection, clouds, the boundary layer, etc. In the simulations used here, described by Watterson et al. (1997), the model includes a slab ocean with prescribed heat fluxes. Thirty years of equilibrated $1 \times CO_2$ and $2 \times CO_2$ climates are analyzed.

The simulated present general circulation is generally similar to that of the Mark 1 model, for which wind and variability statistics were described by Watterson et al. (1995), except that the westerlies in the northern summer are more realistic. The model continues to have

a cold bias in the mid- and low-latitude troposphere and the mean westerly jets tend to be a few degrees equatorward of observed positions. Overall, CSIRO9 compares well with similar climate models (Intergovernmental Panel on Climate Change 1995, hereafter IPCC 1995). The mean surface warming simulated for a doubling of CO_2 is 4.3 K, a sensitivity toward the high end of the range that the Intergovernmental Panel on Climate Change considers realistic (IPCC 1995).

For the present study, the 8-h sigma-level atmospheric data archive from the simulations has been used to construct sea level pressure and geopotential. The former is an extrapolation from surface pressure based on the second sigma level temperatures (approximately 600-m altitude). The height field at 500 hPa is calculated using the assumption that virtual temperature is linear in log(sigma).

3. Weather system identification and tracking

Automated cyclone and anticyclone finding and tracking is used to establish contemporary cyclone behavior, verify that it is realistically simulated by the GCM, and to assess how storminess might change under doubled CO_2. Cyclone identification is based on the scheme of Sinclair (1994), as modified by Sinclair (1997). Only a brief overview is presented here, with discussion only of features relevant to the present GCM application. Unlike many previous studies that locate cyclones as pressure minima, cyclones are here identified as local maxima of gradient-wind cyclonic vorticity as computed from gridded 1000-hPa geopotential (Sinclair 1997). Cyclones identified as pressure minima can vanish when the background pressure gradient increases (Sinclair 1994). Vorticity, on the other hand, can include all mobile disturbances in the westerlies that contribute to transient eddy activity, even those lacking a pressure minimum because of a superimposed pressure gradient. A general reduction in the strength of the polar vortex as expected in a warmer climate would result in detection of more of the pressure minima as an artifact of the reduced meridional pressure gradient. As a kinematic quantity, vorticity is also better related than pressure to eddy transports and to socially important impacts such as strong wind, cloudiness, and precipitation. Vorticity on a coarse grid (as here) is also directly related to circulation. We thus view a ''cyclone'' as a region of cyclonic circulation.

Anticyclones are identified as local maxima of high pressure, as in other studies (Jones and Simmonds 1994; Sinclair 1996). As a counterpoint to cyclones representing storminess, anticyclones here represent ''settled'' dry spells. Changes in their frequency and geographic distribution thus might be expected to impact land use and drought frequency. As discussed by Sinclair (1996), anticyclonic vorticity maxima are mostly found within the storm track as mobile ridges rather than near the broad regions of light winds found near pressure maxima. Thus, to best differentiate anticyclones and their associated settled weather from the storminess of cyclones, we continue the traditional practice of locating anticyclones as pressure maxima.

The datasets used for this study are on different latitude–longitude grids and have decreasing east–west grid spacing toward the poles. The CSIRO9 output was provided at a resolution of around 3.2° lat × 5.6° long and the ECMWF at 2.5° × 2.5°. Because of the scale-dependence of vorticity, the raw higher-resolution ECMWF dataset will admit more vorticity extrema of greater intensity compared with the coarser GCM data. Some model intercomparison studies spectrally filter data to a common lat–long grid to avoid this problem (Gates et al. 1999). This reduces discrepancies resulting from the different grid geometries but retains the disadvantage of an effective decrease in zonal grid spacing toward the poles. Here, we use a constant-radius spatial smoother to ensure that a fixed length scale is consistently admitted before interpolating to a common polar stereographic computational domain. As shown by Sinclair (1997), omitting this smoothing step engenders a high-latitude bias (as large as 400%) in cyclone statistics on the lat–long grid.

The smoother follows Cressman (1959) and averages geopotential data at each grid point with all neighboring points at a distance $r < r_0$ using Gaussian-like weights $(r_0^2 - r^2)/(r_0^2 + r^2)$. A smoothing radius ($r_0$) of 800 km was used here. This is larger than the largest grid spacing on the GCM grid, but small enough to avoid excessive smoothing of already coarse GCM data. After smoothing, results are interpolated to a common computational grid—one for each hemisphere. The computational domain was a 61 × 61 grid on a polar stereographic projection of resolution 221 km at 30° lat.

To demonstrate that smoothing followed by interpolation to a common grid minimizes differences arising from the different domains, we first interpolated a series of 500 particularly noisy high-resolution analyses of 1000-hPa geopotential to the ECMWF and CSIRO grids, and computed gridpoint statistics for cyclonic geostrophic vorticity exceeding 1 CVU.[1] The high-resolution analyses were on a Southern Hemisphere (SH) polar stereographic projection of resolution 80 km at 30°S. Figure 1a confirms that the higher resolution ECMWF grid admits higher counts of strong cyclonic vorticity, with an rms value of cyclonic vorticity over the grid of 14.06 CVU on the ECMWF grid compared with 9.83 CVU on the coarser CSIRO grid. Many very high vorticity values are found near the pole because of the decreasing east–west grid spacing of the latitude–longitude grid (see Fig. 1 of Sinclair 1997). After smoothing with $r_0 = 400$ then a separate run at 800 km

[1] 1 CVU (cyclonic vorticity unit) $= -1 \times 10^{-5}$ s^{-1} in the Southern Hemisphere and 1×10^{-5} s^{-1} in the Northern Hemisphere.

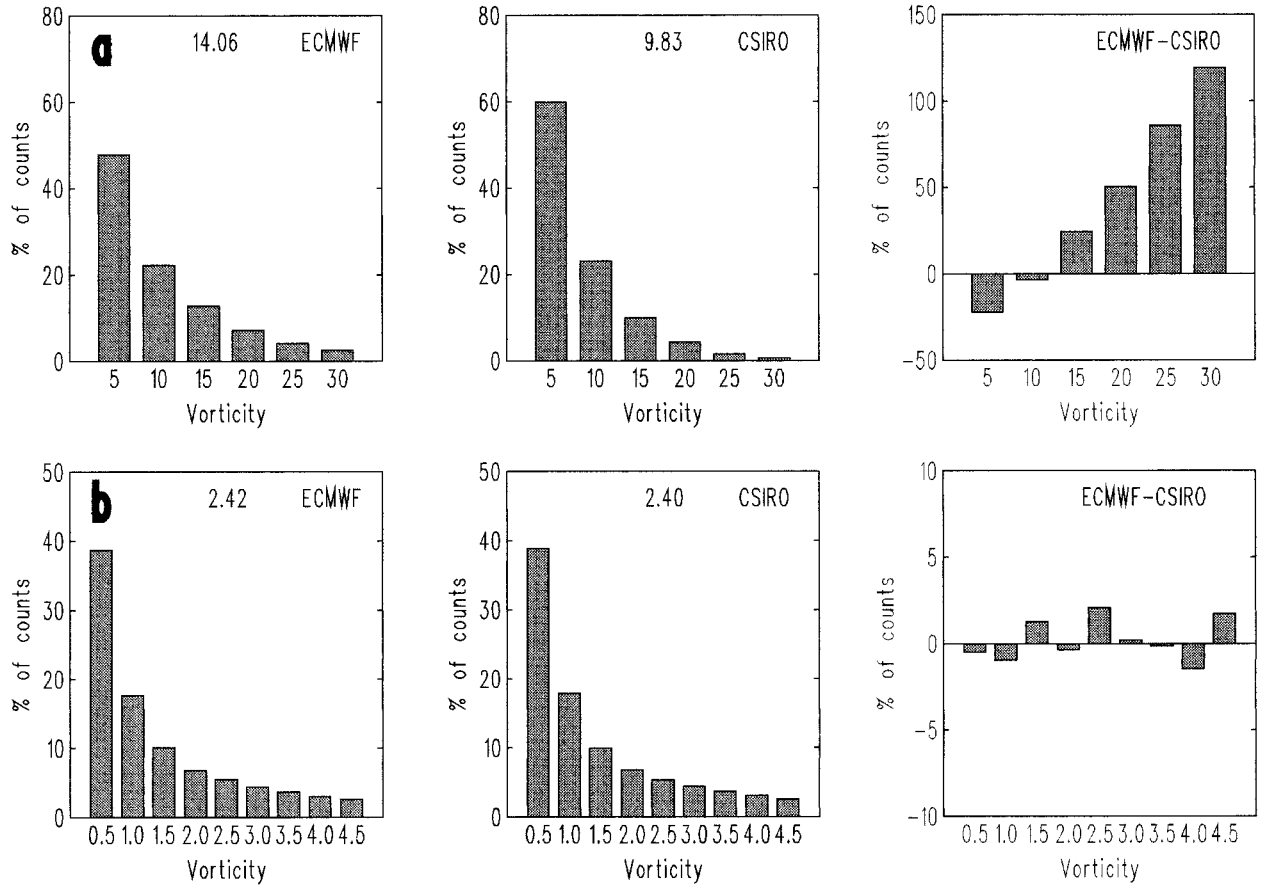

FIG. 1. (a) Frequency distribution for cyclonic vorticity exceeding 1 CVU on the ECMWF grid, the CSIRO grid, and the difference between the two, expressed as a percentage of the actual value. (b) As in (a) except after smoothing with r_0 = 800 km and interpolation to the computational grid.

(not shown), rms cyclonic vorticity values over the grid decrease and become increasingly similar, −6.91 (5.80) CVU for the ECMWF (CSIRO) grid at 400 km and 3.73 (3.39) at 800 km. However, when the actual procedure used for this study is mimicked—smoothing at 800 km followed by interpolation to the polar stereographic computational domain, rms values were found to differ by less than 1% (Fig. 1b). Separate tests showed that most of the vorticity intensity distribution differences between the two grids were eliminated by the interpolation to the common grid; however, omitting the prior spatial smoothing step retains the low-latitude bias of the polar stereographic grid (Sinclair 1997).

Following smoothing, cyclones are identified as local maxima of 1000-hPa cyclonic gradient wind vorticity exceeding 1 CVU while anticyclones are located as local mean sea level pressure maxima. Bicubic spines are used to locate these centers more accurately between grid points, as detailed in Sinclair (1994). Only centers poleward of 20° lat are included as the validity of the gradient wind approximation becomes questionable closer to the equator. Over high terrain where pressure reductions to sea level are uncertain, weather system detection is inhibited by progressively increasing the threshold for detection for terrain elevation over 1000 m. This check is based on a fixed orography file and prevents detection of 1000-hPa features over the Tibetan region, the Rockies, and Greenland in the NH, and over Antarctica, the Andes, and parts of southern Africa for the SH.

The results of cyclone and anticyclone findings at a single CSIRO9 analysis time for both hemispheres are shown in Fig. 2. Cyclones comprise a mixture of closed (marked with a "C") and open (no pressure minimum, "X") centers. High centers are marked with an "H." Two cyclonic vorticity maxima over the Himalayas (Fig. 2a) and one each over the Andes and west Africa (Fig. 2b) are not included (annotated) as they occur over high terrain.

Tracking is based on the scheme of Murray and Simmonds (1991a). Tracking attempts to match cyclones at the current time with centers obtained for the next analysis time 12 h later. For each center, a prediction of the position, pressure, and vorticity for the next track position is made from past motion, pressure, and vorticity tendency. Then a match is attempted between each of

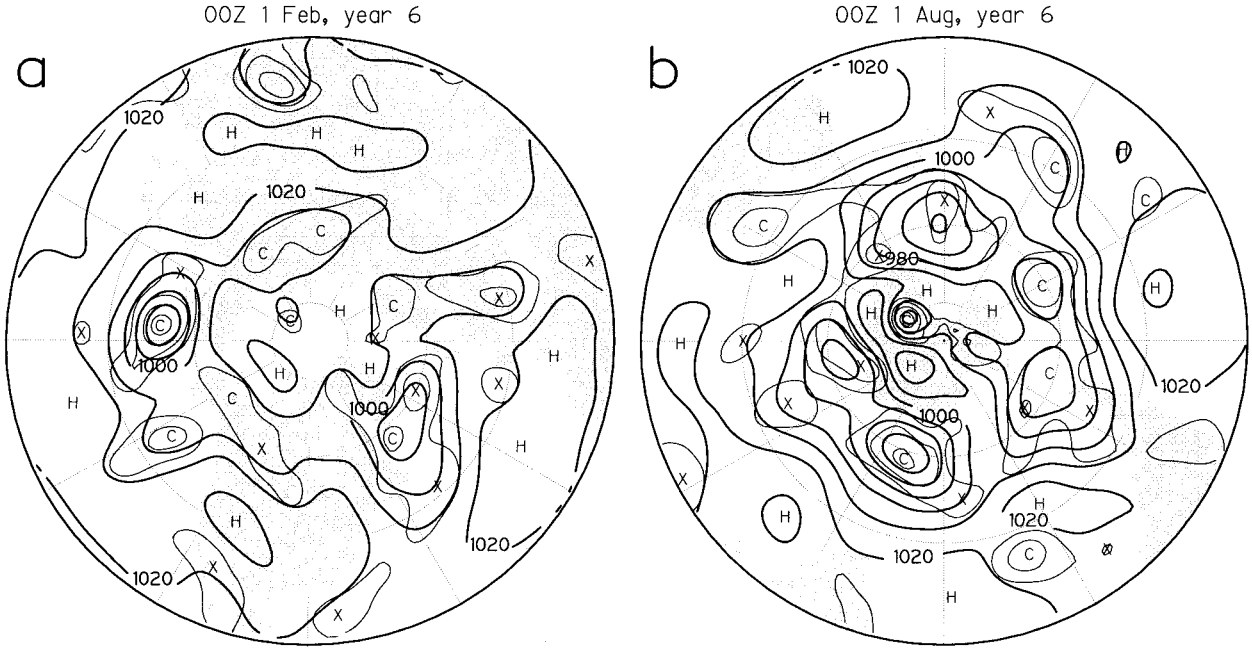

FIG. 2. MSL pressure (solid, every 5 hPa) and cyclonic geostrophic vorticity (thin solid, every 1 CVU) from CSIRO9 GCM control simulation for (a) 0000 UTC 1 February, year 6 for the NH, and (b) 0000 UTC 1 August, year 6 for the SH. Cyclonic vorticity maxima are marked either ''C'' (closed center associated with a pressure minimum) or ''X'' (open center). High centers are marked with ''H.'' Vorticity contour labels are omitted for brevity.

these predictions and the available centers at the next analysis time. The combination of matches chosen is the one that minimizes a weighted sum of absolute departures of location, pressure, and vorticity from predicted values. More details are found in Murray and Simmonds (1991a) and Sinclair (1994).

Cyclone and anticyclone counts are accumulated in circular areas of radius 555 km (5° latitude) that are centered on each grid point of the domain. Circular averaging geometry avoids biases associated with rectangular latitude–longitude boxes (Taylor 1986). Counts are then normalized by dividing by the number of analyses per day (two for ECMWF; three for CSIRO9) then by the number of months included. Resulting counts represent the number of daily systems per area per month.

A preliminary count of all NH cyclonic centers obtained from ECMWF is shown in Fig. 3a. These are similar to Petterssen (1956) and Lambert (1995). Unfortunately, well-known features like the North Pacific and Atlantic storm tracks (e.g., Wallace et al. 1988; Lau 1988) are masked by additional localized maxima over regions like southern California, northern Africa, and southern Asia, well away from the midlatitude storm tracks. Examination of individual synoptic charts reveals that these maxima arise largely from stationary features such as heat lows and lee troughs. Since a goal of this study is to assess how midlatitude storminess might change under global warming scenarios, it is desirable to eliminate these centers from the cyclone statistics. This is done by requiring cyclones over or within 500 km of land to have a total translation as tracked of at least 1200 km. This results in a 40% reduction in the overall number of centers identified. However, virtually all this reduction occurs over land regions, resulting (Fig. 3b) in better definition of the storm track regions. For anticyclones, a similar check is performed to eliminate spurious highs resulting from stationary orographically induced pressure ridges or fictitious pressure reduction to 1000 hPa. Slow-moving systems like blocks that ultimately move off should not be affected. Weather system statistics for the remainder of this study are based on the set of remaining migratory cyclones and anticyclones, along with pressure and vorticity at each track point.

Table 1 shows summary statistics for tracked cyclones and anticyclones from ECMWF (7 yr for the NH and 16 for the SH) and the 1 and 2 $\times$ CO_2 30-yr runs of the CSIRO9 GCM. Overall hemispheric frequencies (tracks per day) and average system lifetimes are fairly consistent across the different data sources. However, there is a higher frequency of NH cyclones from ECMWF compared with both GCM simulations, and slightly fewer systems from the 2 $\times$ CO_2 runs relative to 1 $\times$ CO_2. By applying identical processing to each dataset, we have sought to ensure that these differences reflect intrinsic properties of the datasets. Clearly, observational uncertainty and changes to the analysis procedure and data availability in the ECMWF dataset will also contribute to these differences. We will now ex-

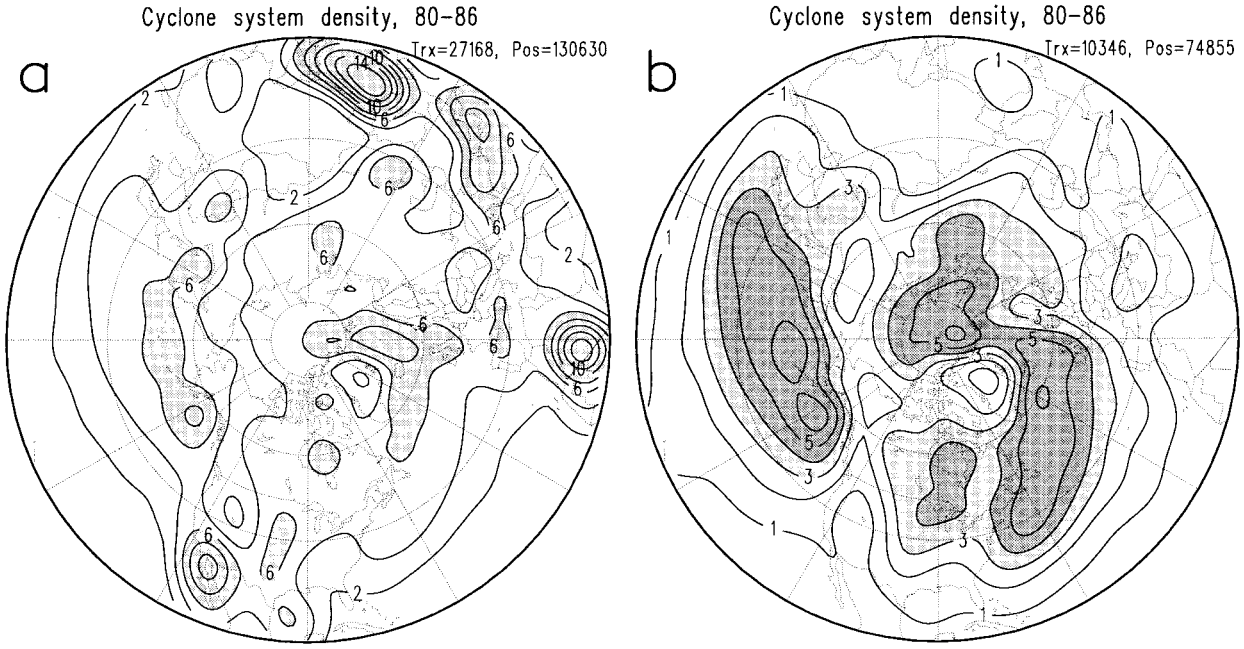

FIG. 3. ECMWF cyclone system density for the NH for the years 1980–86. The ''Trx'' and ''Pos'' values at the top right of each panel refer, respectively, to the numbers of cyclones (as tracked) and positions (centers) used for each plot. (a) All centers included, drawn with a contour interval of 2 centers per 5° lat circle per month (b) quasi-stationary orographic features excluded, every 1 center per 5° per month.

amine the geographical and intensity characteristics of these differences in more detail.

4. Evaluation of the CSIRO9 control weather system climatology

In this section, cyclone and anticyclone statistics are constructed from a 30-yr CSIRO9 GCM equilibrium simulation of the present climate and compared with statistics obtained from ECMWF analyses of observed data. The goal of this section is to determine the degree to which the GCM replicates observed weather system behavior and to illustrate that robust comparison of weather system statistics can be made between these two datasets, despite their differing grid geometries and resolutions.

a. Mean circulation

Because cyclones and anticyclones tend to form where the mean circulation favors their growth, we first evaluate the ability of the GCM to replicate the mid-tropospheric circulation. Figure 4 shows the long-term 500-hPa geopotential height and 1000–500-hPa thickness climatology from CSIRO9, along with difference fields from a climatology based on observational data produced by the National Centers for Environmental Prediction (NCEP). Although the weather system statistics shown in this study are based on ECMWF analyses, NCEP data are used in Fig. 4 because ECMWF 500-hPa data were not available. For brevity, just the annual means are presented here. The NCEP climatology (not shown, but similar to the CSIRO means in Figs. 4a,c,e,g) was constructed from monthly mean

TABLE 1. Weather system statistics for cyclones and anticyclones from ECMWF, $1 \times CO_2$, and $2 \times CO_2$, from both hemispheres, for all systems lasting 2 or more days as tracked. Track numbers, average lifetime (days), and numbers of tracks per day are shown for each category.

	Cyclones						Anticyclones					
	NH			SH			NH			SH		
Hem	No. of tracks	Life (day)	No. day^{-1}	No. of tracks	Life (day)	No. day^{-1}	No. of tracks	Life (day)	No. day^{-1}	No. of tracks	Life (day)	No. day^{-1}
ECMWF	7045	4.4	2.8	16 797	4.5	2.9	3491	4.9	1.4	6438	5.7	1.1
$1 \times CO_2$	25 397	4.7	2.3	32 411	4.8	3.0	15 258	5.0	1.4	14 543	5.1	1.3
$2 \times CO_2$	23 686	4.8	2.2	29 750	5.0	2.7	14 693	5.0	1.3	13 715	5.2	1.2

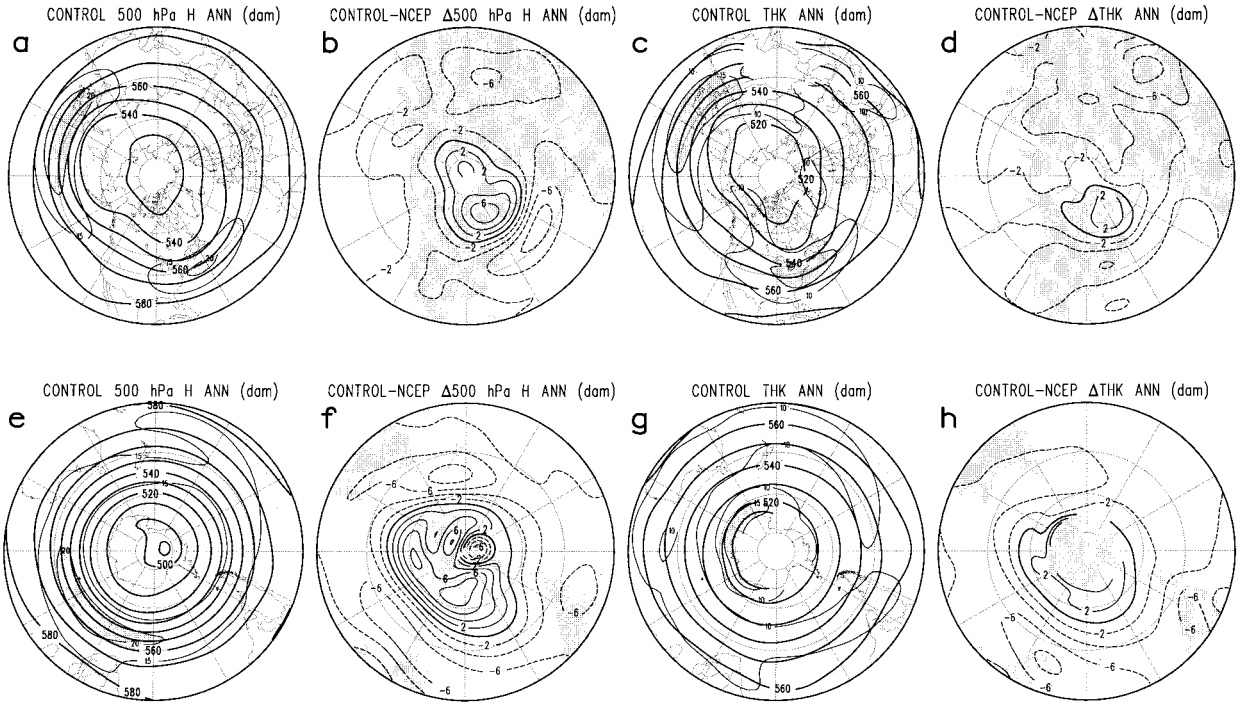

FIG. 4. (a) Mean annual NH 500-hPa height (solid, every 10 dam) with 15 and 20 m s^{-1} geostrophic wind speed contours added (>20 m s^{-1} shaded) from CSIRO9 GCM control simulation. (b) Control minus NCEP height (every 2 dam). (c)–(d) As for (a)–(b) except for 1000–500-hPa thickness, with thermal wind in excess of 15 m s^{-1} shaded. (e)–(h). As for (a)–(d) except for SH.

fields of reanalysis data spanning 1979–95 and is based on a fixed, state-of-the-art numerical analysis methodology incorporating all available observations (Kalnay et al. 1996). A comparison for the SH (not shown) revealed that the time-averaged 500-hPa height field from ECMWF differed from NCEP by less than 2 dam over the hemisphere, with a domain-average rms difference of around 0.5 dam. For the difference fields in Fig. 4, the *t* statistic based on the 17 NCEP and 30 CSIRO9 annual mean fields indicated that differences exceeding ±1–2 dam are statistically significant at the 5% level for both hemispheres, for both geopotential (Figs. 4b,f) and thickness differences (Figs. 4d,h).

Statistically significant GCM biases are found that are consistent with those described by Watterson et al. (1995) for the Mark 1 model, based on comparison with a shorter (5-yr) series of ECMWF analyses. The CSIRO9 control simulation underestimates the strength of the polar vortex in both hemispheres (Figs. 4b,f), with polar (midlatitude) regions more than 6 dam too high (low). As a result of this weakened polar vortex, geostrophic westerlies in the North Atlantic and southern Indian Ocean are more than 6 m s^{-1} too low (not shown). However, the CSIRO9 westerlies extend farther into the Tropics, with westerly geostrophic wind anomalies equatorward of about latitude 40 in both hemispheres (not shown). Thickness fields (Figs. 4c,d and 4g,h) have a similar structure, with a GCM warm bias in polar regions and a cold bias elsewhere, especially over land (Figs. 4d,h). This decreases the mean baroclinicity in many midlatitude regions, especially near Labrador (Fig. 4d) and over much of the southern Indian and Atlantic Oceans (Fig. 4h). These CSIRO9 climate errors have an impact on weather system behavior in this GCM, as we now see.

b. Cyclones

Figure 5 compares the geographic distribution of cyclones obtained from ECMWF and CSIRO9. To exclude ephemeral systems and enable determination of properties like translation velocity and vorticity tendency that require more than one track point, only cyclones tracked for two or more days are used. Cyclones at all stages of development are included. For brevity, just annual means are presented. The measure of cyclone activity used here is ''track density,'' defined as the number of discrete cyclone tracks passing within 555 km (5° lat) of any point per month. It is obtained by counting centers just once per track per grid point. The more commonly used measure of cyclone activity is system density (Fig. 3), which is a simple count of centers without regard to tracking. This produces noisier fields and high counts of slower-moving systems such as those in the Aleutian and Icelandic regions (e.g., Fig. 3b). While these may be of interest in some contexts, we have chosen to use track density, which yields a more coherent cyclone distribution highlighting migra-

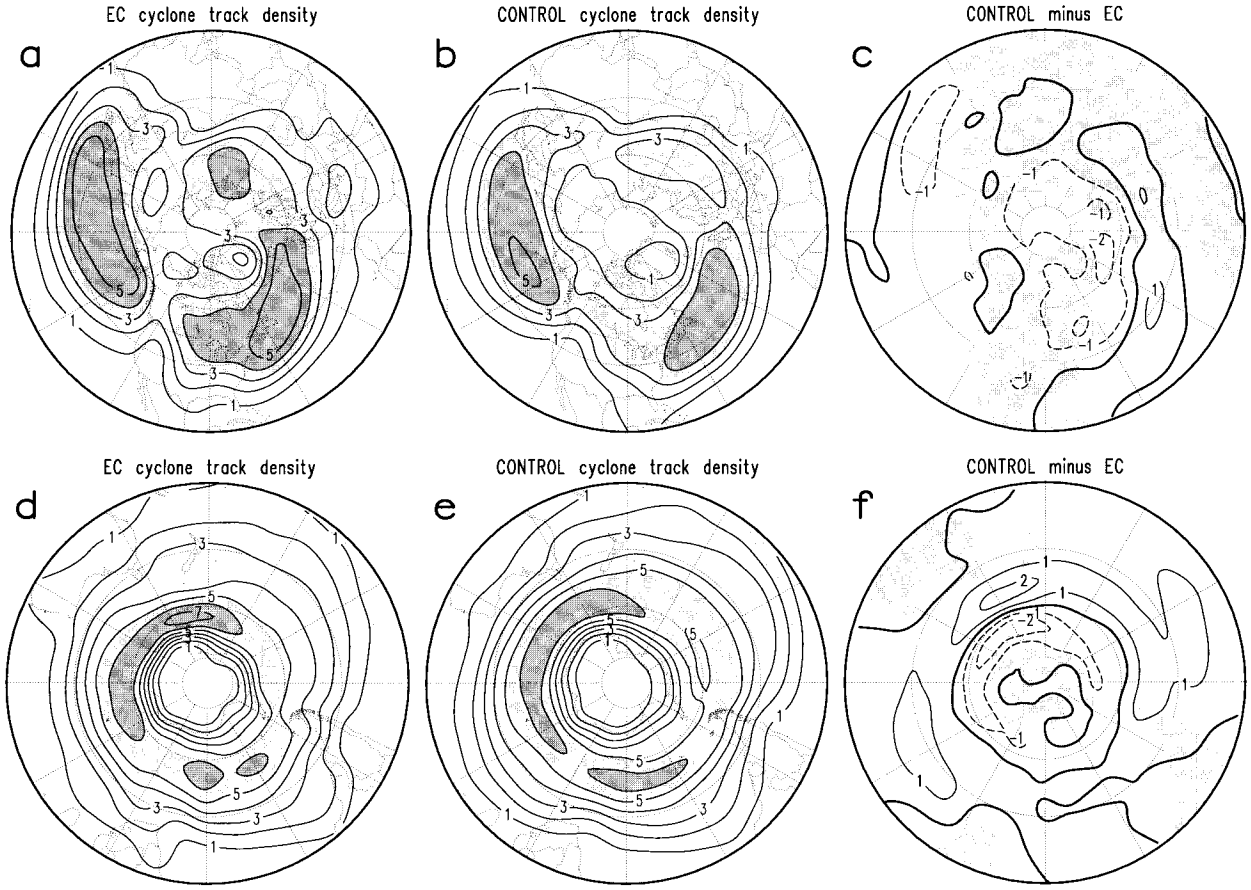

FIG. 5. Cyclone track density for the NH every 1 center per 5° lat circle per month, with values >3 and 4 shaded, for (a) ECMWF and (b) control. (c) Difference control minus ECMWF, contour interval 1 center per 5° lat circle per month. (d)–(f) As for (a)–(c) except for SH. Only cyclones lasting 2 or more days are included.

tory weather systems that occur within the baroclinic storm track regions of the globe (Fig. 5).

ECMWF results for the NH (Fig. 5a) reveal two main storm tracks—one in the North Pacific extending from Japan toward the Gulf of Alaska and the other extending from North America across the North Atlantic and into the Arctic Ocean. These maxima straddle, and extend downstream from, the regions of strongest time-averaged baroclinicity in Fig. 4c. Other maxima occur east of the Urals and over the Mediterranean Sea. The patterns in Fig. 5a are similar to highpass-filtered variance statistics derived by Wallace et al. (1988) and Lau (1988), to cyclone track density charts constructed manually by Whittaker and Horn (1984) and to recent results of Sinclair (1997) based on an automated procedure similar to that used here. The reader is referred to these publications for further interpretation and discussion of contemporary NH cyclone statistics and their seasonality.

Results from CSIRO9 (Fig. 5b) confirm this general picture of cyclone activity, but with slightly reduced numbers of cyclones compared with observations overall, particularly just poleward of the two principal storm tracks. Differences in mean track density exceeding ± 1 cyclone per month per 5° circle (the contour interval used in Fig. 5) are statistically significant at the 5% level in both hemispheres, despite the rather short period of observations used in this study. The reduced cyclone activity is consistent with the smaller GCM baroclinicity in these regions (Fig. 4d) and the coarser resolution of the CSIRO9 model. The dipolar difference field in the Atlantic (Fig. 5c) suggests an equatorward shift of the GCM storm track there. Hall et al. (1994), Murphy (1995), and Carnell et al. (1996) noted that the Atlantic storm track maximized too far south in their GCM simulations, with the storm track penetrating too far into western Europe. However, Senior (1995) finds that this error is reduced for simulations at higher resolution.

Southern Hemisphere results are presented in Figs. 5d–f. The ECMWF results are in reasonable agreement with bandpass-filtered variance statistics obtained by Trenberth (1991), satellite-based statistics compiled by Carleton (1979) and Streten and Troup (1973), and with track density statistics derived by Sinclair (1995). Maximum cyclone numbers are found south of the climatological polar jet stream axis (Fig. 4e), particularly near

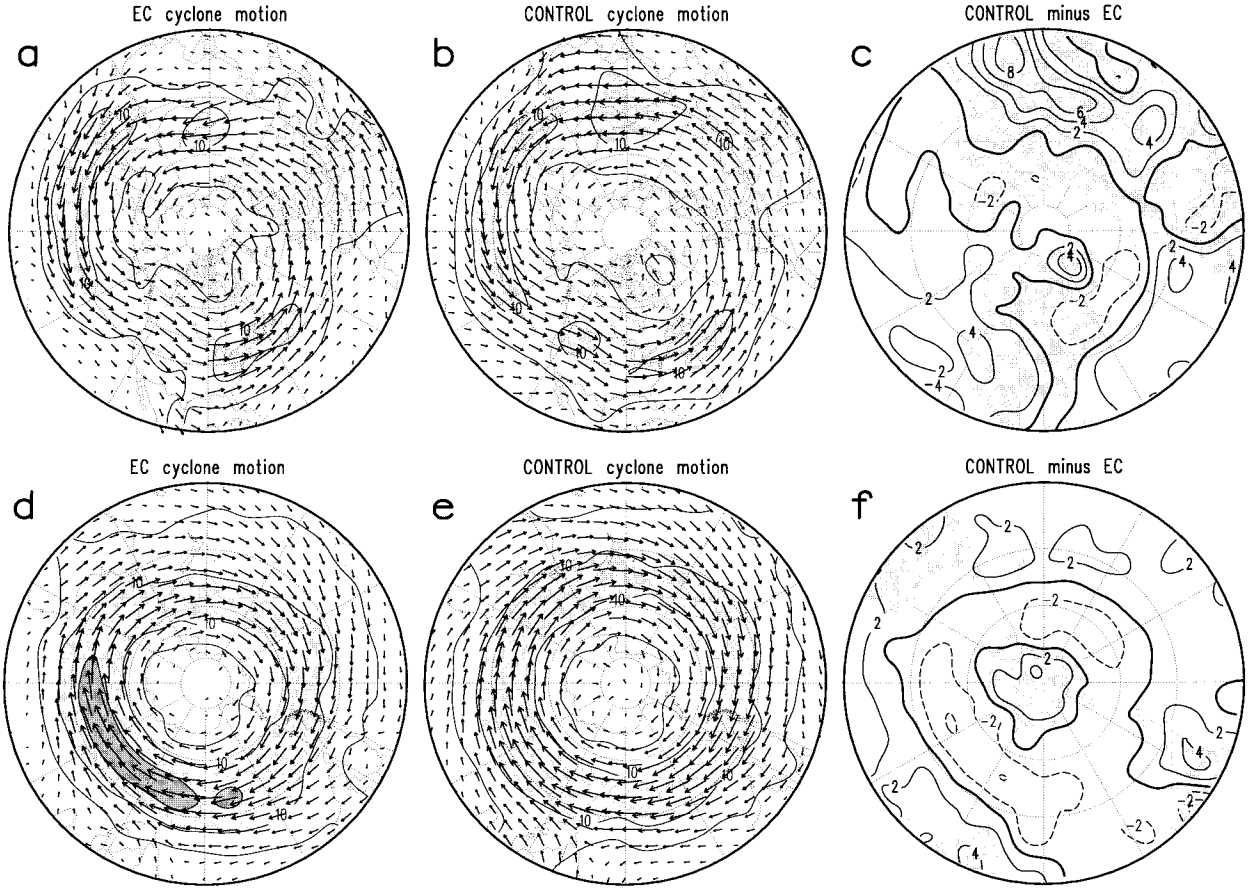

FIG. 6. Average annual cyclone motion vectors and speed contours (every 5 m s^{-1}, values >10 shaded) for the NH for (a) ECMWF and (b) control. (c) Control minus ECMWF cyclone translation speed difference field (every 2 m s^{-1}). (d)–(f) As for (a)–(c) except for SH.

its exit region south of New Zealand. There is a hint of a secondary maximum extending across New Zealand from eastern Australia, with a relative minimum near 50°S south of New Zealand. This bifurcation is related to the double jet structure in Fig. 4e. It is better depicted in winter system density plots (e.g., Fig. 4b of Sinclair 1995).

CSIRO9 results for the SH (Fig. 5e) shift the maximum cyclone frequency equatorward (see Fig. 5f) and broaden it, particularly in the South Pacific. A very similar broadening of the SH storm track seen in simulations from a 5° lat × 7.5° long resolution version of the Hadley Centre atmospheric GCM was greatly reduced at 2.5° × 3.75° resolution (Senior 1995).

Mean cyclone motion (Fig. 6) is computed from the cyclone track coordinates using centered time differences. Mobility maximizes in regions of strongest 500-hPa mean flow in the western North Pacific and Atlantic Oceans (Fig. 4a) and Indian Ocean (Fig. 4e). However, there are some systematic biases in the CSIRO9 results, the most notable being a tendency for cyclones to move too fast near elevated terrain (Figs. 6c,f). This probably relates to lower terrain as represented in the CSIRO9 model, which is less able to block the passage of cyclones. There is also a slow (fast) bias at higher (lower) latitudes over oceans in the SH (Fig. 6f) and in the North Atlantic (Fig. 6c). These motion errors appear consistent with the reduced strength of the GCM polar vortex and the greater equatorward extent of the extratropical westerlies in the GCM noted earlier.

We also examined the ability of the GCM to depict rapid cyclogenesis (Fig. 7). Vigorous cyclogenesis involves complex interactions on a variety of scales, along with input of energy from the underlying sea and subsequent release of latent heat. Evaluating a model's ability to depict rapid cyclogenesis thus provides an exacting check on model performance (e.g., Sanders and Mullen 1996). Statistics for winter cyclogenesis (Fig. 7) are accumulated as instances where central vorticity following a track becomes more cyclonic at a rate exceeding 2×10^{-5} s^{-1} $(24\ h)^{-1}$, computed as a centered difference. At the resolution used, this subset includes around 2%–5% of all centers (depending on the hemisphere and dataset used) at the rapid cyclogenesis end of the intensity change spectrum.

The main winter cyclogenesis regions for the NH (Fig. 7a) as depicted in the ECMWF dataset are eastern seaboards of Asia and North America, consistent with

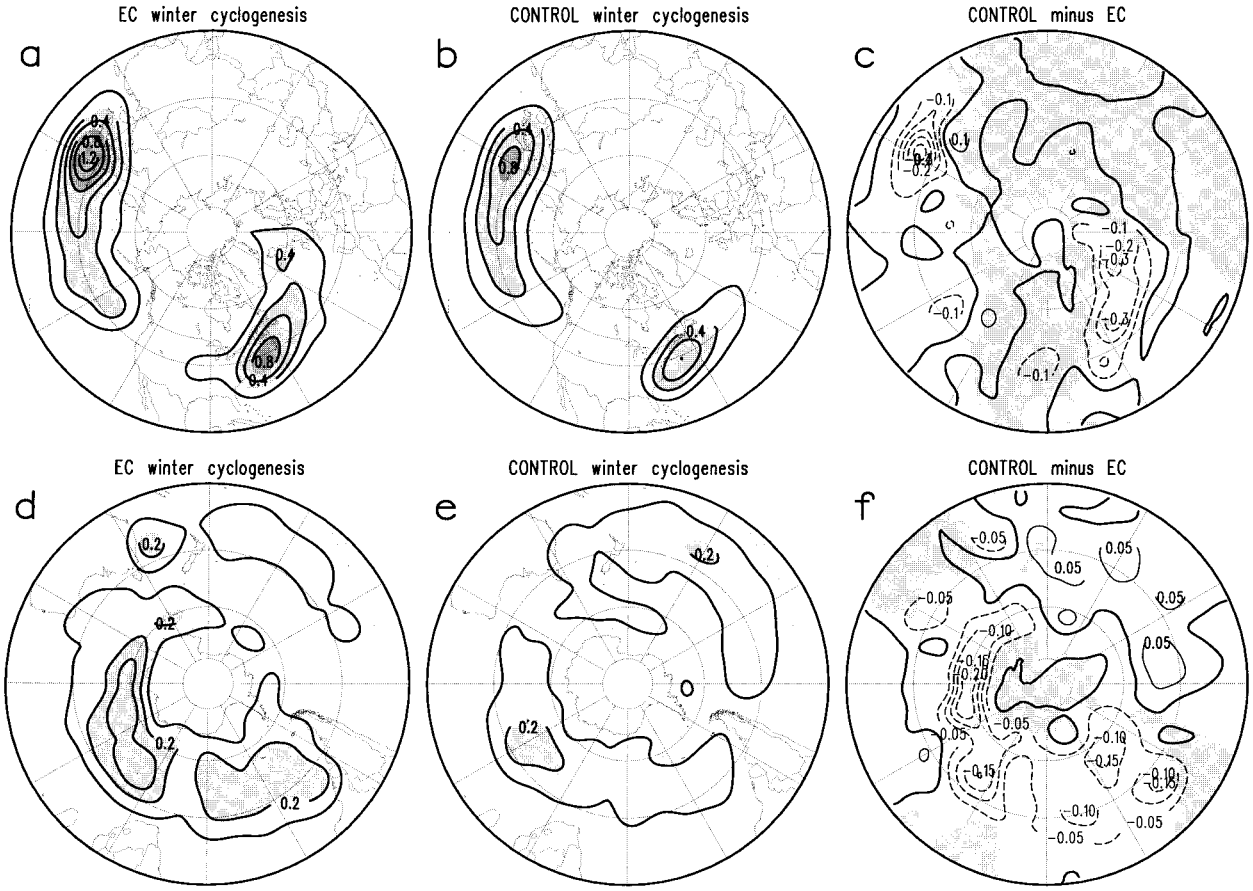

FIG. 7. Counts of instances of cyclonic vorticity increase >2 CVU day^{-1}, every 0.2 centers per 5° lat circle per month, with values >0.4 and 0.8 shaded, for the NH, for (a) ECMWF and (b) control. (c) Difference control minus ECMWF, every 0.1 centers per 5° lat circle per month. (d)–(f) As for (a)–(c) except for SH and the contour interval is 0.1 for (d) and (e) and 0.05 for (f).

statistics obtained by Sanders and Gyakum (1980), Roebber (1984), Gyakum et al. (1989), and Sinclair (1997). Rapid cyclogenesis is less frequent over the SH (Fig. 7d), with maxima east of South America and Australia, across the Pacific near 35°S and in a belt extending across the Indian Ocean from southeast of Africa into high Pacific latitudes. The subtropical branch of the double cyclogenesis maximum in the Pacific is related to the winter subtropical jet (Sinclair 1995). The CSIRO9 GCM (Figs. 7b,e) broadly replicates the regions prone to rapid cyclogenesis, but underestimates its frequency, particularly near the eastern seaboards of both hemispheres (Figs. 7c,f) where strong gradients of SST and enhanced uptake of heat and moisture occur. It is possible that the coarser GCM is unable to resolve the sharp thermal contrasts in these regions. One feature of Fig. 7f is a slightly higher CSIRO9 cyclogenesis frequency over the South Pacific.

Constructing frequency histograms for various vorticity (Figs. 8a–f) and vorticity change (Figs. 8g–l) categories can readily identify systematic biases in cyclone intensity. The CONTROL minus ECMWF difference histograms in Figs. 8e, 8f, 8i, and 8l are expressed as a percentage change for each vorticity category to enable changes in the tails of the intensity distribution to be more easily seen. For ease of comparison, cyclonic vorticity, and vorticity change are depicted as positive in both hemispheres. The latter is computed as a 24-h centered difference.

To assess whether the standard deviations of the distributions in Figs. 8a,b differ significantly, we applied a χ^2 test based on the assumption that 1 in 10 of the center vorticity values are independent. Estimating the number of independent samples is somewhat arbitrary. Clearly, vorticity at a given track point will depend on other values adjacent in both space and time. Here we assert that the vorticity at one point depends on no more than nine other such points, which seems reasonable for the spatial and temporal resolutions used. The histogram in Fig. 8a constructed from 7 yr of ECMWF data incorporates around 10 000 tracked cyclones[2] comprising

[2] More than in Table 1, as Fig. 7 uses all centers, not just ones lasting 2 or more days.

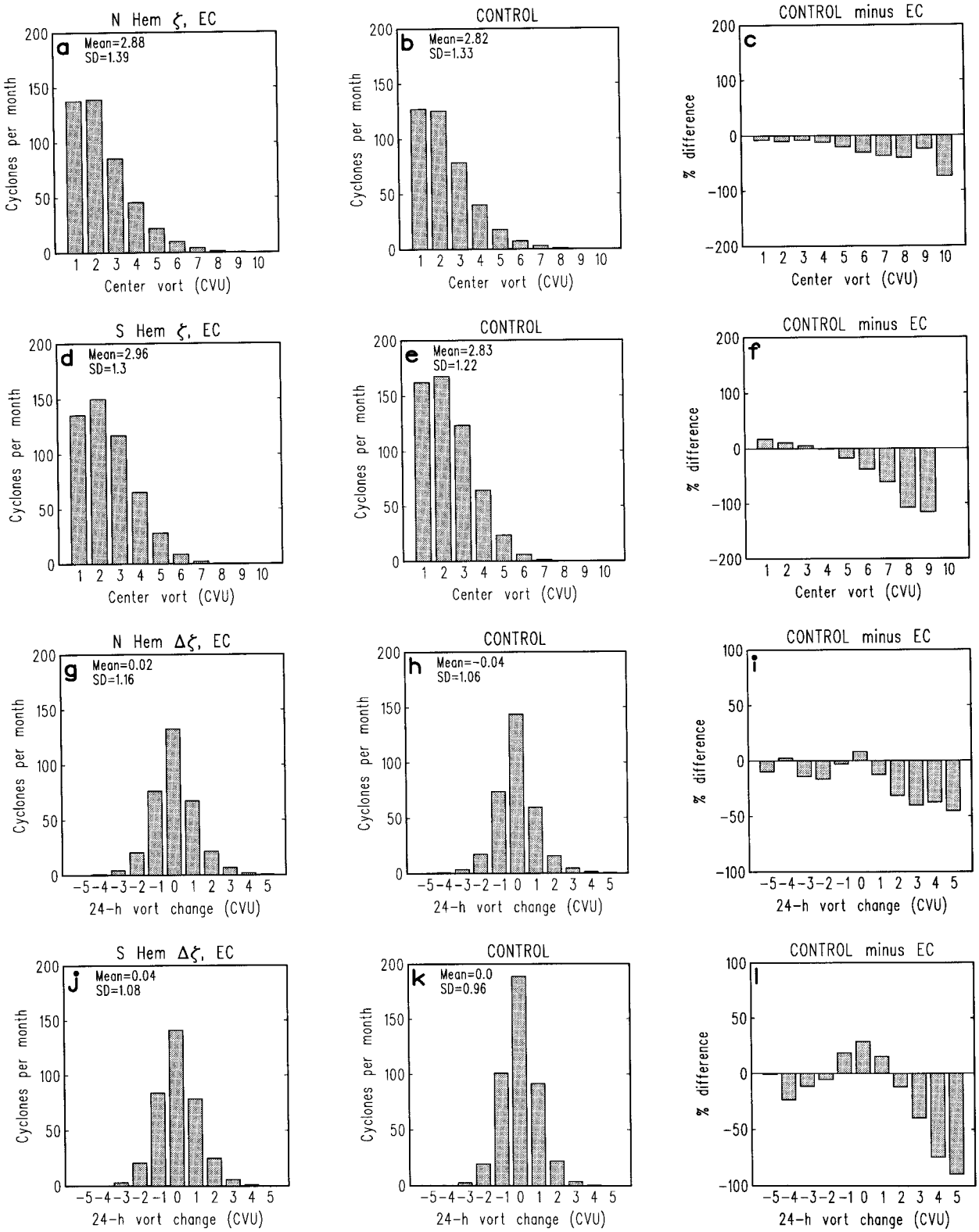

FIG. 8. Frequency distribution of cyclone center vorticity for the NH for (a) ECMWF, (b) control, and (c) control minus ECMWF. (d)–(f) As for (a)–(c) except for SH. The mean and std dev for these distributions are included. (g)–(l) As for (a)–(f) except for 24-h central vorticity change. The column labeled 2 means values ranging from 2.0 to 3.0, etc. These distributions are based on all cyclone centers (those having three or more points for vorticity change).

75 000 track points. The χ^2 test based on 7500 degrees of freedom yields a 95% confidence interval for the standard deviation of 1.37 to 1.41. The 30-yr CSIRO9 control simulation yielded more than 430 000 NH cyclone centers, resulting in a confidence interval for the 1.33 standard deviation of that distribution (Fig. 8b) of smaller than ± 0.01. Thus, the standard deviation's for the distributions in Figs. 8a and 8b do differ significantly at better than the 95% level. Similar calculations for the other histograms in Fig. 8 reveal that the CSIRO9 distributions are consistently narrower than the corresponding ECMWF distributions for both vorticity (cf. Figs. 8a,d with 8b,e) and vorticity change (Figs. 8g,j and 8h,k) at better than the 95% level of statistical significance.

Figure 8 shows that the GCM simulates too few cyclones at the high intensity end of the spectrum (Figs. 8c,f). A similar result is found for intensity *change* (Figs. 8i,l), with 20%–100% fewer CSIRO9 cyclones intensifying faster than about 2 CVU per day. This is consistent with the decreased cyclogenesis counts in Fig. 7. CSIRO9 also produces fewer rapidly *weakening* cyclones, with population increases only for those having almost no intensity change. It should be noted here that the constant-radius spatial smoother reduces the frequency of intense cyclones, particularly from the ECMWF dataset, which is provided at a higher resolution. However, in applying this smoothing, we have ensured that the differences seen in Fig. 8 arise from underlying differences between the observations and the GCM rather than from the geometry of the grids that the data are provided on. Thus, differences seen in Fig. 8 relate to the coarser model grid that the CSIRO9 GCM is run on, which is presumably less able to resolve the strong baroclinic zones, jet streaks, and land–sea discontinuities that are conducive to rapid cyclogenesis. A similar result of underpredicting strong lows and overpredicting weak ones was found by Carnell et al. (1996). We anticipate that this bias toward weaker cyclones would be reduced for a climate model run at a finer resolution.

In summary, the CSIRO9 GCM replicates gross features of the contemporary ECMWF cyclone climatology, but appears to produce slightly fewer and generally weaker cyclones, particularly in the strongly cyclogenetic regions of the globe. These discrepancies mirror GCM circulation errors, particularly in the mean baroclinicity field. Results are broadly consistent with most other GCMs, which generally tend to underestimate the strength of the observed storm track (Hall et al. 1994; Murphy 1995; IPCC 1995). According to Senior (1995), these errors in storm track depiction diminish at higher resolution. Thus, many of the errors reported here are probably related to the coarse resolution of the CSIRO9 model.

c. Anticyclones

Anticyclone statistics are accumulated from counts of tracked high pressure centers. In the NH, highs are most frequent (Fig. 9a) in a belt spanning the North Pacific between 30° and 40°N, over a broader region of North America centered on the Great Lakes and extending into the North Atlantic, and near Mongolia. These maxima lie just equatorward of the main NH storm track (Fig. 5a) and are consistent with hemispheric compilations by Petterssen (1956), and Zishka and Smith (1980) and Harman (1987) for the North American region. Very few highs are found in the Gulf of Alaska and near Iceland. These regions are instead home to large numbers of decaying cyclones (Roebber 1984; Sinclair 1997). The CSIRO9 model (Fig. 9b) replicates these features, but underestimates anticyclone frequency near Japan and North America while overestimating it over central Asia (Fig. 9c).

In the SH (Fig. 9d), highs occur between 30° and 40°S, well equatorward of the main cyclone storm track between 55° and 65°S (Fig. 5d), a region where highs are very rare. Stationary highs over Antarctica are all but eliminated via the mobility requirement near land. More discussion of contemporary SH anticyclone behavior is found in Taljaard (1967), Jones and Simmonds (1993), and Sinclair (1996). CSIRO9 results (Fig. 9e) are in good agreement with these observed patterns, but with slight underestimation near maxima and too many highs in the Pacific sector.

The frequency distribution of anticyclone center pressure is shown in Fig. 10. In the NH (Figs. 10a–c), the CSIRO9 model yields too many intense highs and undercounts weak ones (Fig. 10c). This is consistent with the mean surface pressure bias plot for the NH (not shown), which reveals a high sea level pressure bias in most of the regions that anticyclones are found (Figs. 9a,b). This GCM bias is reversed in the SH (Fig. 10f), with the CSIRO9 model giving more (fewer) weak (intense) anticyclones, compatible with an underestimation (overestimation) of low- and mid- (high) latitude surface pressure by the GCM (not shown, but similar to Fig. 4f).

5. Impact of climate change

a. Mean circulation

To identify this GCM's response to greenhouse warming, we compare mean fields and weather system statistics from 1 and 2 $\times$ CO_2 simulations from the CSIRO9 model. Figure 11 shows annual means for 500-hPa geopotential height and thickness for 2 $\times$ CO_2 runs, along with 2 $\times$ CO_2 minus 1 $\times$ CO_2 difference fields. The 1 $\times$ CO_2 (control) fields are omitted, but are qualitatively similar to the doubled CO_2 results. The difference fields show global-scale increases for the greenhouse simulation in both 500-hPa geopotential (Figs. 11b,f) and thickness (Figs. 11d,h) in both hemispheres. These rises range from about 8 dam in the subtropics to more than 13 dam in polar regions and are somewhat magnified near land. Quantitatively, these changes are

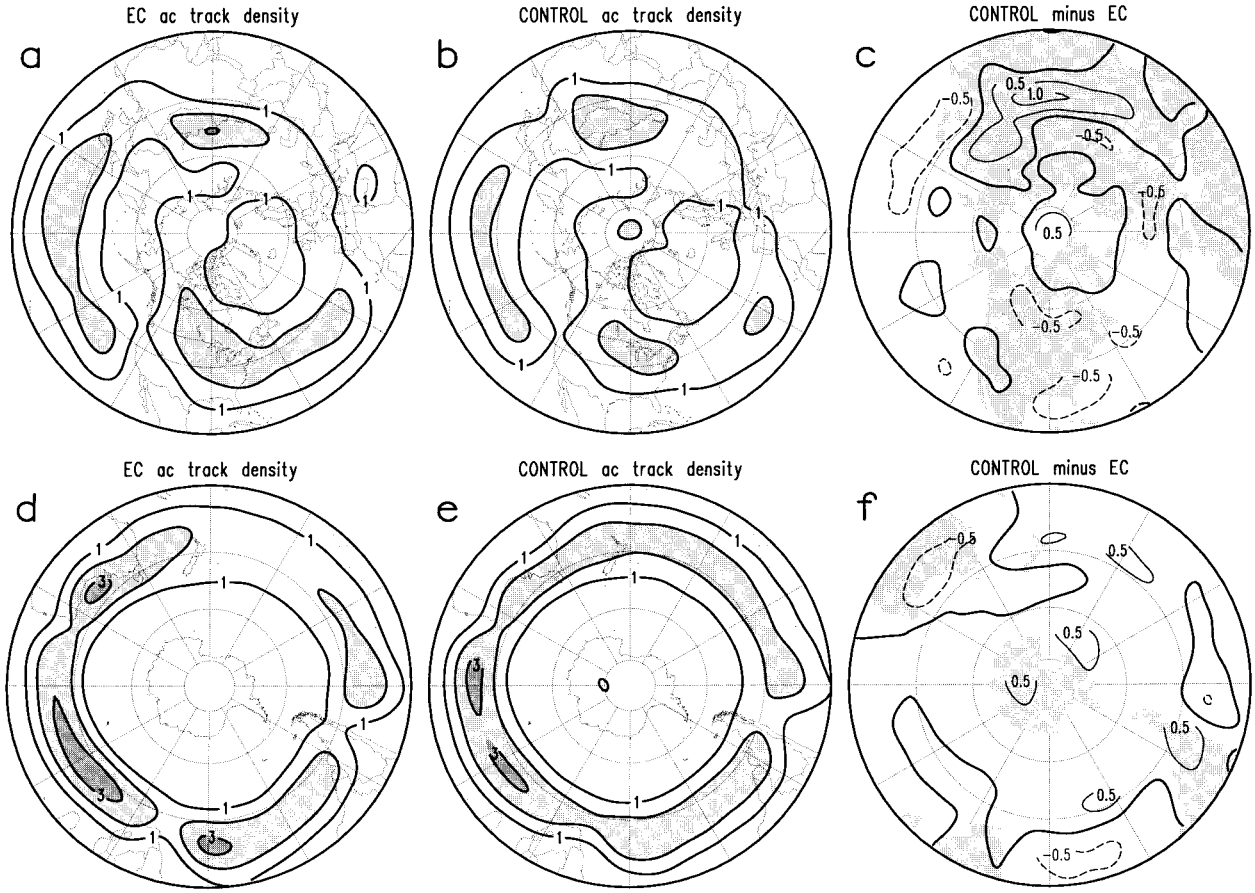

FIG. 9. Anticyclone track density for the NH every 1 center per 5° lat circle per month, with values >2 and 3 shaded, for (a) ECMWF and (b) control. (c) Difference control minus ECMWF, every 0.5 centers per 5° lat circle per month. (d)–(f) As for (a)–(c) except for SH. Just anticyclones lasting 2 or more days are included.

larger than the corresponding control versus observed differences in Figs. 4b,d,f,h. However, associated changes in the *gradients* of these quantities (not shown), representing wind and baroclinicity changes, are somewhat smaller than for the observed versus control comparison in Fig. 4 (note the smaller contour interval in Fig. 11). Compared with the $1 \times CO_2$ simulation, the $2 \times CO_2$ atmosphere exhibits weaker westerlies (Figs. 11b,f) and less baroclinicity (Figs. 11d,h) throughout most of the extratropics of both hemispheres. Reduced baroclinicity is particularly marked in the North Atlantic (Fig. 11d), while over southern Europe, there are small increases in both meridional thickness gradient and the strength of the westerlies.

These circulation changes are qualitatively similar to those found in other studies and to the doubled CO_2 response of the Mark 1 version of the CSIRO GCM (Watterson et al. 1995). While differing in details, the weakened westerlies, reduced meridional temperature gradient, and patterns of tropospheric warming maximizing at high latitudes and over land feature in all GCM simulations of greenhouse response (IPCC 1995). As a first approximation, the reduced equator-to-pole temperature gradient would suggest a reduction in midlatitude storm activity, although localized increases in average baroclinicity and enhanced water vapor content in a warmer atmosphere might be expected to increase storm activity in some regions. We now examine the weather system response to doubled CO_2.

b. Extratropical weather system response

Changes in winter cyclone and anticyclone frequency under greenhouse warming as simulated by the CSIRO9 GCM are shown in Fig. 12. Winter results only are shown here for brevity and to facilitate comparison with other studies. The $1 \times CO_2$ (control) cyclone track density field for the NH (Fig. 12a) is qualitatively similar to the annual field found in Fig. 5b except for a strengthening of the two storm tracks. The SH storm track (Fig. 12e) extends farther into lower latitudes than the all-month result in Fig. 5e, with a better-defined double maximum in the South Pacific. These storm track locations match regions of rainfall computed for this GCM by Watterson (1998).

Difference fields (Figs. 12b,f) show mostly dimin-

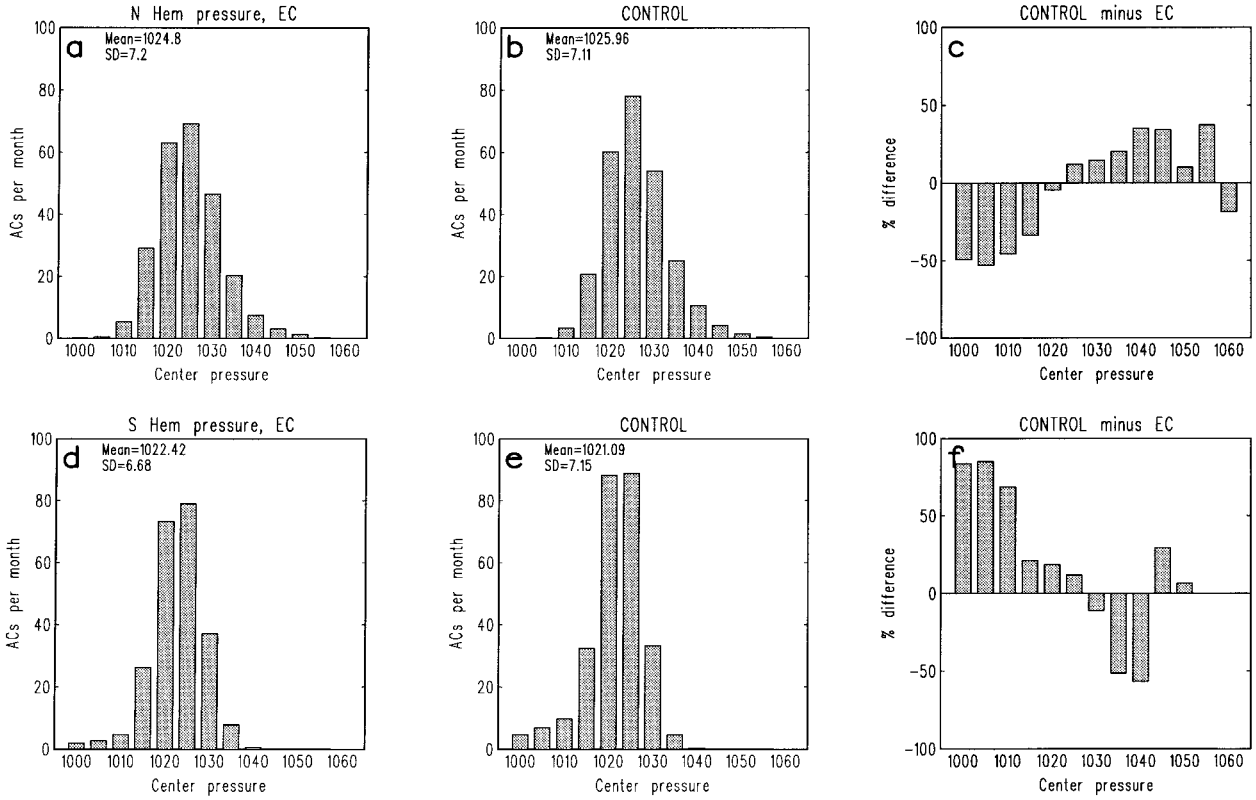

FIG. 10. Frequency distribution of anticyclone center pressure (hPa) for the NH for (a) ECMWF, (b) control, and (c) control minus ECMWF. (d)–(f) As for (a)–(c) except for SH. The mean and std dev for these distributions are included.

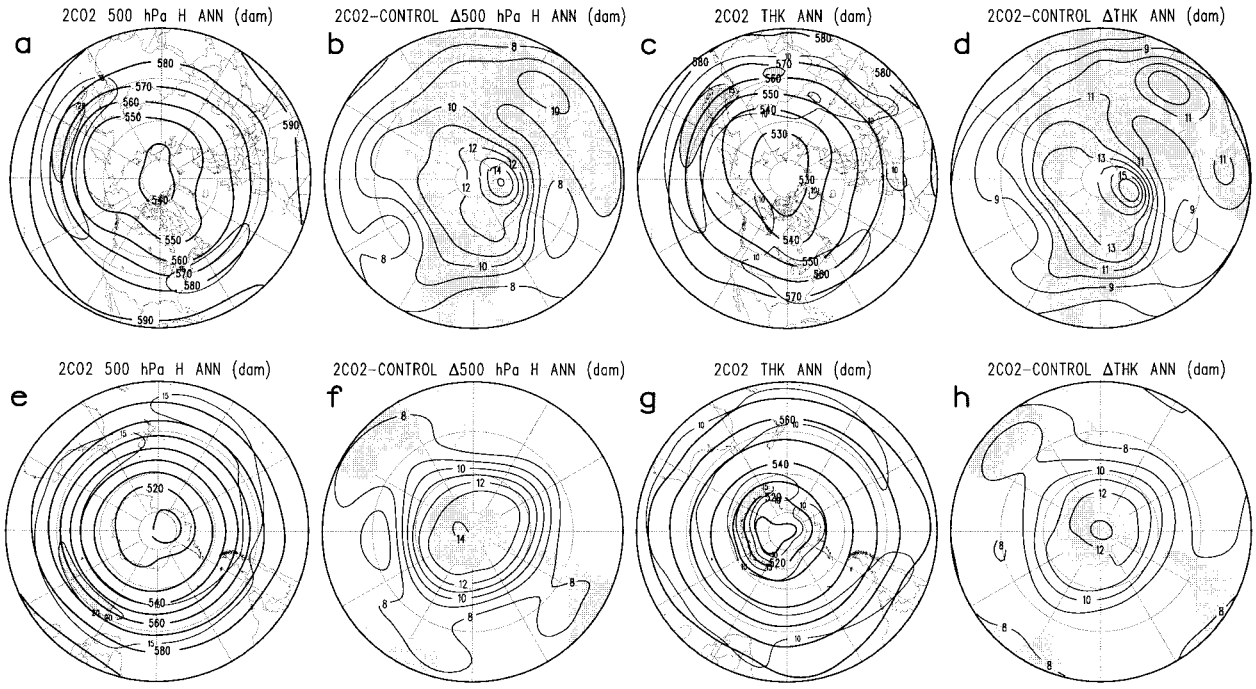

FIG. 11. CSIRO9 greenhouse climate response. (a) Mean annual NH 500-hPa height (solid, every 10 dam) with 15 and 20 m s^{-1} geostrophic wind speed contours added (>20 m s^{-1} shaded) from 2 × CO_2 simulation. (b) 2 × CO_2 minus 1 × CO_2 (every 1 dam). (c)–(d) As for (a)–(b) except for 1000–500-hPa thickness, with thermal wind in excess of 15 m s^{-1} shaded. (e)–(h) As for (a)–(d) except for SH.

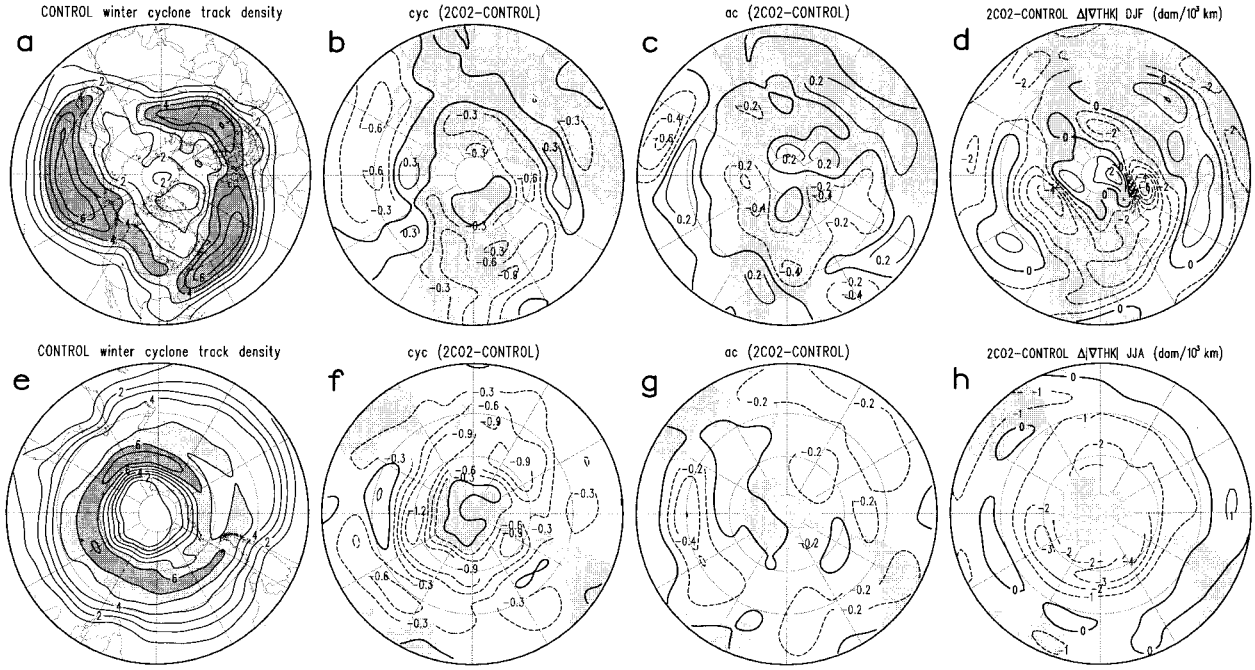

FIG. 12. CSIRO9 greenhouse weather system response. (a) Cyclone track density for the NH winter (Dec–Feb) every 1 center per 5° lat circle per month, with values >3 and 4 shaded, for 1 × CO_2. (b) 2 × CO_2 minus 1 × CO_2 cyclone track density difference, every 0.3 centers per 5° lat circle per month. (c) As for (b) except for anticyclones and contour interval 0.2. (d) 2 × CO_2 minus 1 × CO_2 change in the gradient of 1000–500-hPa thickness, every 1 dam (1000 km)$^{-1}$. (e)–(h) As for (a)–(d) except for SH winter (Jun–Aug). Just systems lasting 2 or more days are included.

ished cyclone activity for the 2 × CO_2 simulation. For the NH (Fig. 12b), decreases of 10%–15% largely follow the storm track. However, some regional increases are seen, particularly over southern Europe, near the downstream end of the Atlantic storm track, and west of North America at the end of the North Pacific storm track. Over the SH (Fig. 12f), decreases in cyclone activity are found over the entire hemisphere, except for a small increase southwest of Australia.

The mean track density fields for anticyclones are omitted for brevity, but are qualitatively similar to those in Fig. 9. Changes in NH winter anticyclone frequency under greenhouse warming (Fig. 12c) are more complex than for cyclones, with reduced activity over North America and east of Asia, but increases over subtropical landmasses and in midocean. Generally decreased occurrence of highs is seen over the SH (Fig. 12g). Finally, the motion of both cyclones and anticyclones (not shown) is 1–2 m s^{-1} slower for the 2 × CO_2 run, particularly in the SH extratropics and near the main NH storm track.

This greenhouse weather system response tends to mirror changes in tropospheric baroclinicity (Figs. 12d,h). Thickness gradients and cyclone activity are both generally reduced near the main storm tracks in both hemispheres. In the NH, increased cyclone and anticyclone activity over the eastern ends of the Pacific and Atlantic storm tracks (Figs. 12b,c) corresponds with increased baroclinicity in those regions. Watterson et al. (1995) found changes in high-pass transient eddy kinetic energy in the lower troposphere similar to Fig. 12b in the Mark 1 version of the present model. There, the increases over Europe occurred mostly in winter, peaked in the upper troposphere, and coincided with a downstream extension of the upper-level jet in that region. These appeared to result from changed advection patterns in this region. Watterson (1998) also showed increases in rainfall for the Mark II version of the model over British Columbia, the Aleutian region, and near Spain that closely match the increases in Fig. 12b. The moisture for this increased rainfall was supplied by changes in the advection by the mean flow rather than the eddies. A further analysis (not shown) for the present study showed that latent heating coincides with the rainfall, with the maximum in the lower troposphere (near 800 hPa).

Hall et al. (1994) identified a similar eastern intensification of the North Atlantic storm track, along with consistent changes in time-averaged features such as the Eady growth rate and the upper-level jet, although the increases over Europe were farther north than in Fig. 12b. Senior (1995) finds that increases in transient eddy activity at the end of the storm track are more apparent at higher resolution, as they are barely seen in a coarser resolution version of the U.K. Meteorological Office (UKMO) model. The resolution of the present model is between the two UKMO versions studied by Senior, so the modest changes over Europe in Fig. 12 appear con-

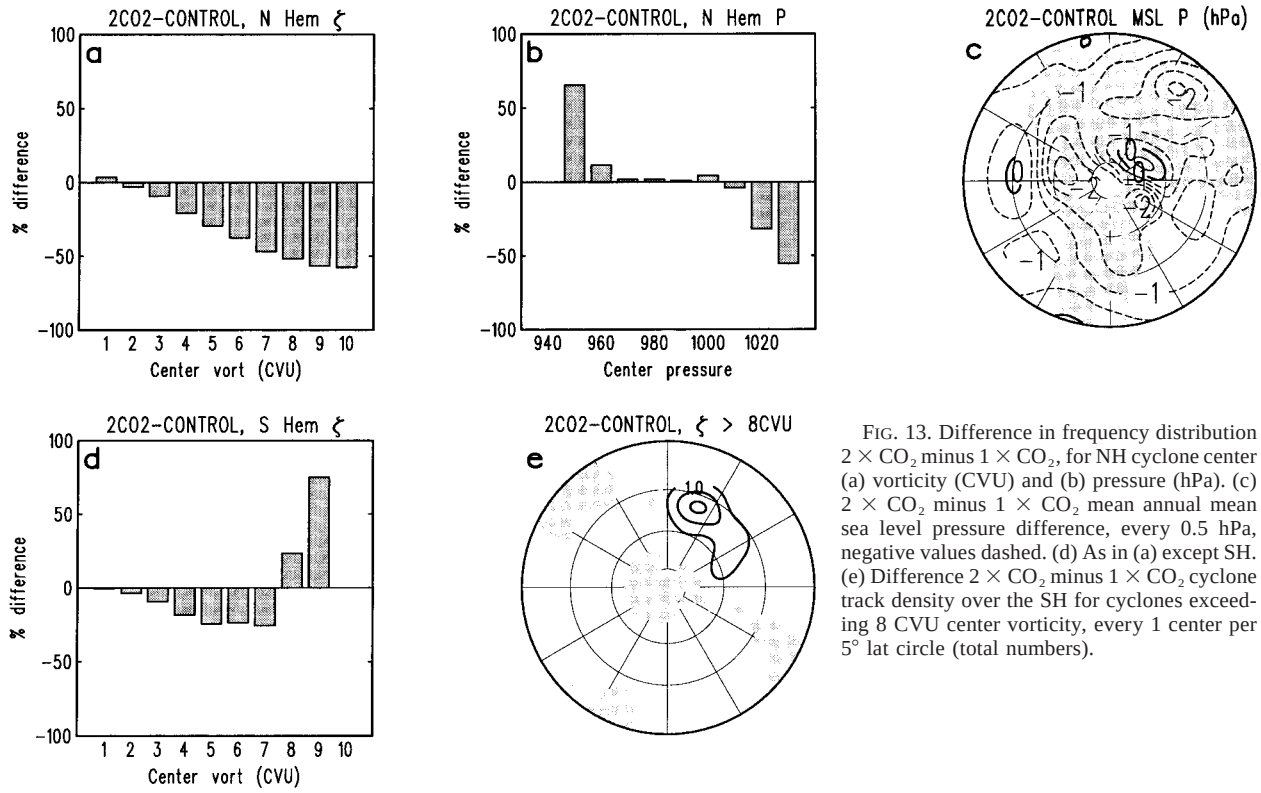

FIG. 13. Difference in frequency distribution $2 \times CO_2$ minus $1 \times CO_2$, for NH cyclone center (a) vorticity (CVU) and (b) pressure (hPa). (c) $2 \times CO_2$ minus $1 \times CO_2$ mean annual mean sea level pressure difference, every 0.5 hPa, negative values dashed. (d) As in (a) except SH. (e) Difference $2 \times CO_2$ minus $1 \times CO_2$ cyclone track density over the SH for cyclones exceeding 8 CVU center vorticity, every 1 center per 5° lat circle (total numbers).

sistent with the UKMO results, although here, the changes are located farther south. Zhang and Wang (1997), using a coarse (R15) version of the NCAR Community Climate Model failed to detect any increases at all. Instead, they identified a general reduction for the NH in both eddy activity and Eady growth rate.

Previous studies using both transient eddy statistics and explicit cyclone tracking algorithms have failed to find coherent patterns of change in cyclone frequency, despite mutually consistent and coherent changes in both eddy statistics and baroclinicity. For example, Carnell et al. (1996) found increases in transient eddy activity at the end of the North Atlantic storm track similar to Hall et al. (1994), yet failed to find consistent changes when low pressure centers were counted directly. Similarly, Zhang and Wang (1997) found a noisy mixture of increases and decreases in cyclone frequency in response to global warming, despite decreases in both Eady growth rate and transient eddy activity. König et al. (1993) also found a noisy cyclone response to greenhouse warming, with bandpass eddy variance peaking equatorward of the cyclone frequency maxima.

Discrepancies in these studies between eddy statistics and direct counts of synoptic systems appear to arise from the requirement for cyclones to exhibit a local pressure minimum. As Carnell et al. (1996) note, this yields maximum cyclone activity poleward of the variance maxima because of the tendency for pressure minima to locate poleward of the corresponding streamfunction extrema. More importantly, large numbers of mobile vorticity centers that contribute to the transient eddy variance actually go undetected because they do not exhibit a pressure minimum (Sinclair 1994), biasing cyclone detection in favor of regions of weaker pressure gradients away from the strongest westerlies. Because of the reduced meridional pressure gradient under global warming (Fig. 11), this bias would contribute an artificial *increase* in ''cyclone'' counts, masking any real decrease in transient eddy activity. Here, because of our use of vorticity in place of pressure minima, we find a coherent greenhouse cyclone response (Fig. 12) that is consistent with changes in both baroclinicity (Fig. 11) and eddy statistics.

c. *Changes in cyclone intensity*

To conclude our study of climate change response for the CSIRO9 GCM, we examine possible cyclone intensity changes under $2 \times CO_2$ (Fig. 13). Clearly, any potential change in the intensity of midlatitude storms is of great interest to society. A key question is how the occurrence of *intense* storms might change under doubled CO_2. The histograms in Fig. 13 address this issue. In the NH (Fig. 13a), there are fewer cyclones in all but the weakest intensity band, with substantial decreases in the frequency of intense storms. Vorticity *change* statistics (not shown) also confirm this picture,

with fewer rapidly changing (intensifying or decaying) systems under doubled CO_2.

These results are in contrast with those of Lambert (1995), who claimed that a $2 \times CO_2$ run of the Canadian Climate Centre GCM gave an increased frequency of intense NH cyclones compared with the control climatology. However, Lambert used 1000-hPa central height values as a proxy for cyclone intensity. A similar compilation for the CSIRO9 model (Fig. 13b) yielded results similar to those of Lambert, with increased population of cyclones having lower central pressure for the $2 \times CO_2$ run. Here, the changes in Fig. 13b are due to shifts in the background surface pressure climatology and not to any real increase in the intensity of storms under greenhouse warming. This is evident from Fig. 13c, which shows average surface pressure 1–3 hPa lower throughout much of the NH under greenhouse warming, consistent with the increased numbers of cyclones having central pressure below about 1000 hPa (Fig. 13b). According to Sinclair (1995, 1997), central pressure alone is not a reliable measure of cyclone intensity. At the coarse resolutions used in this study, central vorticity (as used in Fig. 13a) provides a superior indication of the strength of a cyclone's inner circulation. The differing inferences from Figs. 13a and 13b underscore the necessity of ensuring that suitable measures of storm intensity are used to define changes in extreme events.

In the SH, the $2 \times CO_2$ simulation exhibited a decreased incidence of cyclones stronger than about 2 CVU (Fig. 13d), as in the NH. However, there is an increase in the frequency of very intense storms (>8 CVU) under greenhouse warming. These storms occur between 40° and 60°S in the South Pacific (Fig. 13e) and occur almost exclusively in late summer (not shown) in the enhanced greenhouse run, implying that increased latent heating might be an underlying cause for this increase. However, as they occur on average only 2–3 times per year in the $2 \times CO_2$ simulation (less in the control run), a longer simulation is necessary to confirm this to be a robust feature of the GCM's enhanced CO_2 climate.

The question of whether storms will increase in frequency or intensity in response to greenhouse warming is complex. While most earlier GCMs suggest decreased eddy activity overall, higher-resolution runs of coupled atmosphere and ocean GCMs are starting to report regional variations, with some increases, particularly at the downstream ends of storm tracks such as over western Europe. On the one hand, virtually all GCM greenhouse simulations report decreased zonally averaged baroclinicity resulting from patterns of low-tropospheric warming that maximize near the poles. On the other hand, the release of additional latent heat produces maximum warming of the upper troposphere that peaks in the Tropics. This may imply an enhanced available potential energy source aloft. Furthermore, the increased availability of moisture in a generally warmer atmosphere may increase the likelihood of occasional storms of extraordinary vigor. These competing processes make answers to these questions difficult. Carnell et al. (1996) propose a longer observational record to provide more robust statistics of present-day storms combined with higher-resolution runs of state-of-the-art GCMs using more realistic climate change scenarios to answer these perplexing questions.

6. Concluding remarks

A synoptic-climatological approach based on automated weather system identification and tracking has been used to assess the skill of the CSIRO9 GCM in replicating contemporary cyclone and anticyclone behavior, and to estimate possible changes as a result of doubled CO_2. Weather system behavior in the GCM atmosphere was first compared against that obtained from an observational dataset from ECMWF. Migratory cyclone and anticyclone centers were identified and tracked via an objective method, and statistics accumulated to identify regions of persistent weather system activity. A constant-radius spatial smoother was applied to each dataset before interpolating to a common computational grid. Experiments showed that this procedure virtually eliminated differences arising from the different grid configurations.

Locating cyclones as cyclonic vorticity maxima instead of pressure minima avoided any bias related to the strength of the westerlies, as pressure minima can vanish as the background pressure gradient increases. Difference maps helped highlight shifts in storm track locations and intensity between datasets, while frequency histograms for various storm intensity and intensity change categories were used to identify systematic model biases in storm strength.

Climatologies of cyclone and anticyclone behavior based on observational data were in good agreement with previously published statistics. The control simulation of the CSIRO9 GCM realistically reproduced the observed storm tracks, but with a slight reduction in overall cyclone numbers and a bias toward weaker cyclones. The incidence of intense cyclogenesis is strongly underestimated, especially near eastern seaboards where cyclones receive enhanced heat and moisture input from the underlying ocean. This underestimation of weather system activity is compatible with that found in other GCMs of comparable resolution. According to Senior (1995), reductions in the horizontal resolution of these GCMs should reduce these errors. Walsh and Watterson (1997) found similar limitations in the depiction of tropical cyclones in the CSIRO9 model. Apparently, intense vortices are underrepresented in statistics from GCMs of modest resolution. Unfortunately, in assessing the impacts from climate change, these are the most important to be able to predict.

Comparisons between 1 and $2 \times CO_2$ simulations are used to identify possible changes in atmospheric cir-

culation and weather system behavior as a result of doubled CO_2. As in previous GCM studies, maximum increases in both 500-hPa geopotential height and 1000–500-hPa thickness were found at higher latitudes, leading to a weakening of the westerlies and their baroclinicity in most areas except near the end of the NH storm tracks. Coherent changes in cyclone and anticyclone activity consistent with these circulation changes were found, including increases in cyclone activity near the downstream ends of the storm tracks. Previous studies that locate cyclones as pressure minima failed to find any meaningful correspondence between measures of baroclinicity and transient eddy statistics on the one hand, and direct counts of low centers on the other. Because of the weaker background pressure gradient, these studies probably overestimate cyclone counts for doubled CO_2. Our use of vorticity to locate cyclones ensured that changes in cyclone frequency were consistent with both circulation changes and eddy statistics computed by Watterson et al. (1995).

Doubled CO_2 leads to a marked decrease in the occurrence of intense storms as deduced from central vorticity. One exception is over the South Pacific where there is a suggestion of an increased incidence of cyclones at the intense end of the spectrum. Reductions in average cyclone central pressure that have been used in other studies to promote the possibility of enhanced storminess under greenhouse warming, are more likely the result of global-scale sea level pressure falls rather than any real increase in cyclone circulation strength. Such discrepancies underscore the need to ensure that measures of cyclone activity and intensity are realistic and do not introduce bias. Unlike many previous studies, the synoptic identification procedures outlined here yield results that are dynamically consistent with features of the time-averaged circulation and with transient eddy statistics.

This study has highlighted the serious differences that remain between various GCM projections of how storminess might change under doubled CO_2. Confident statements about this issue must await better consensus between several of the most up-to-date, coupled atmosphere–ocean models. The objective weather system identification and tracking procedures outlined here can be used to validate these GCMs against observational data and to intercompare their assessments of how weather system behavior might change under future climate scenarios. Explicit tracking offers the ability to separate contributions from cyclones and anticyclones, of being able to stratify results by intensity and to assess how climate change might impact the duration, motion, intensity, and intensification rates of weather systems.

Acknowledgments. Gridded atmospheric analyses were provided by the ECMWF. The NCEP reanalysis data were extracted by Todd Mitchell of the Joint Institute for the Study of the Atmosphere and Ocean at the University of Washington and made available at the World Wide Web site http://tao.atmos.washington.edu/data_sets/reanalysis/index.html. Funding for Dr. Sinclair was from the New Zealand Foundation for Research, Science and Technology. Dr. Watterson's work contributes to the CSIRO Climate Change Research Program, in part funded by Australia's National Greenhouse Research Program. Our thanks also to Martin Dix for extracting the GCM data used here.

REFERENCES

Akyildiz, V., 1985: Systematic errors in the behaviour of cyclones in the ECMWF operational models. *Tellus,* **37A,** 297–308.

Bell, G. D., and L. F. Bosart, 1989: A 15-year climatology of Northern Hemisphere 500 mb closed cyclone and anticyclone centers. *Mon. Wea. Rev.,* **117,** 2142–2163.

Blackmon, M. L., Y.-H. Lee, and J. M. Wallace, 1984: Horizontal structure of 500 mb height fluctuations with long, intermediate and short time scales. *J. Atmos. Sci.,* **41,** 961–979.

Blender, R., K. Fraedrich, and F. Lunkeit, 1997: Identification of cyclone-track regimes in the North Atlantic. *Quart. J. Roy. Meteor. Soc.,* **123,** 727–741.

Carleton, A. M., 1979: A synoptic climatology of satellite-observed extratropical cyclone activity for the Southern Hemisphere winter. *Arch. Meteor. Geophys. Bioklimatol.,* **27B,** 265–279.

Carnell, R. E., C. A. Senior, and J. F. B. Mitchell, 1996: An assessment of measures of storminess: Simulated changes in Northern Hemisphere winter due to increasing CO_2. *Climate Dyn.,* **12,** 467–476.

Cressman, G. P., 1959: An operational objective analysis system. *Mon. Wea. Rev.,* **87,** 367–374.

Dean, D. B., and L. F. Bosart, 1996: Northern Hemisphere 500-hPa trough merger and fracture: A climatology and case study. *Mon. Wea. Rev.,* **124,** 2644–2671.

Gates, W. L., 1992: AMIP: The Atmospheric Model Intercomparison Project. *Bull. Amer. Meteor. Soc.,* **73,** 1962–1970.

——, and Coauthors, 1999: An overview of the results of the Atmospheric Model Intercomparison Project (AMIP 1). *Bull. Amer. Meteor. Soc.,* **80,** 29–55.

Gordon, H. B., and S. P. O'Farrell, 1997: Transient climate change in the CSIRO coupled model with dynamic sea ice. *Mon. Wea. Rev.,* **125,** 875–907.

Gyakum, J. R., J. R. Anderson, R. H. Grumm, and E. L. Gruner, 1989: North Pacific cold season surface cyclone activity: 1975–1983. *Mon. Wea. Rev.,* **117,** 1141–1155.

Hall, N. M. J., B. J. Hoskins, P. J. Valdes, and C. A. Senior, 1994: Storm tracks in a high resolution GCM with doubled CO_2. *Quart. J. Roy. Meteor. Soc.,* **120,** 1209–1230.

Harman, J. R., 1987: Mean monthly North American anticyclone frequencies, 1950–79. *Mon. Wea. Rev.,* **115,** 2840–2848.

Hodges, K. I., 1994: A general method for tracking analysis and its application to meteorological data. *Mon. Wea. Rev.,* **122,** 2573–2586.

——, 1996: Spherical nonparametric estimators applied to the UGAMP model integration for AMIP. *Mon. Wea. Rev.,* **124,** 2914–2932.

Hudson, D. A., 1997: Southern African climate change simulated by the GENESIS GCM. *S. Afr. J. Sci.,* **93,** 389–408.

——, and B. C. Hewitson, 1997: Mid-latitude cyclones south of Africa in the GENESIS GCM. *Int. J. Climatol.,* **17,** 459–473.

Intergovernmental Panel on Climate Change, 1995: *Climate Change 1995: The Science of Climate Change.* J. T. Houghton, L. G. Meira Filho, B. A. Callander, N. Harris, A. Kattenburg, and K. Maskell, Eds., Cambridge University Press, 572 pp.

Jones, D. A., and I. Simmonds, 1993: A climatology of Southern Hemisphere extratropical cyclones. *Climate Dyn.,* **9,** 131–145.

——, and ——, 1994: A climatology of Southern Hemisphere anticyclones. *Climate Dyn.,* **10,** 333–348.

Kalnay, E. M., and Coauthors, 1996: The NCEP/NCAR 40-Year Reanalysis Project. *Bull. Amer. Meteor. Soc.*, **77,** 437–471.
Katzfey, J. J., and K. L. McInnes, 1996: GCM simulations of eastern Australian cutoff lows. *J. Climate,* **9,** 2337–2355.
König, W., R. Sausen, and F. Sielmann, 1993: Objective identification of cyclones in GCM simulations. *J. Climate,* **6,** 2217–2231.
Lambert, S. J., 1988: A cyclone climatology of the Canadian Climate Centre General Circulation Model. *J. Climate,* **1,** 109–115.
——, 1995: The effect of enhanced greenhouse warming on winter cyclone frequencies and strengths. *J. Climate,* **8,** 1447–1452.
Lau, N.-C., 1988: Variability of the observed midlatitude storm tracks in relation to low-frequency changes in the circulation pattern. *J. Atmos. Sci.,* **45,** 2718–2743.
Lefevre, R. J., and J. W. Nielsen-Gammon, 1995: An objective climatology of mobile troughs in the Northern Hemisphere. *Tellus,* **47A,** 638–655.
Murphy, J. M., 1995: Transient response of the Hadley Centre Coupled Model to increasing carbon dioxide. Part I: Control climate and flux adjustment. *J. Climate,* **8,** 36–56.
Murray, R. J., and I. Simmonds, 1991a: A numerical scheme for tracking cyclone centres from digital data. Part I: Development and operation of the scheme. *Aust. Meteor. Mag.,* **39,** 155–166.
—— and —— 1991b: A numerical scheme for tracking cyclone centres from digital data. Part II: Application to January and July general circulation model simulations. *Aust. Meteor. Mag.,* **39,** 167–180.
—— and ——, 1995: Responses of climate and cyclones to reductions in Arctic sea ice. *J. Geophys. Res.,* **100** (C), 4791–4806.
Petterssen, S., 1956: *Weather Analysis and Forecasting.* Vol. 1, *Motion and Motion Systems.* McGraw-Hill, 428 pp.
Roebber, P. J., 1984: Statistical analysis and updated climatology of explosive cyclones. *Mon. Wea. Rev.,* **112,** 1577–1589.
Sanders, F., and J. R. Gyakum, 1980: Synoptic-dynamic climatology of the ''bomb.'' *Mon. Wea. Rev.,* **108,** 1589–1606.
——, and S. L. Mullen, 1996: The climatology of explosive cyclogenesis in two general circulation models. *Mon. Wea. Rev.,* **124,** 1948–1954.
Senior, C. A., 1995: The dependence of climate sensitivity on the horizontal resolution of a GCM. *J. Climate,* **8,** 2860–2880.
Simmonds, I., and X. Wu, 1993: Cyclone behaviour response to changes in winter Southern Hemisphere sea ice concentration. *Quart. J. Roy. Meteor. Soc.,* **119,** 1121–1148.
Sinclair, M. R., 1994: An objective cyclone climatology for the Southern Hemisphere. *Mon. Wea. Rev.,* **122,** 2239–2256.
——, 1995: A climatology of cyclogenesis for the Southern Hemisphere. *Mon. Wea. Rev.,* **123,** 1601–1619.
——, 1996: A climatology of anticyclones and blocking for the Southern Hemisphere. *Mon. Wea. Rev.,* **124,** 245–263.
——, 1997: Objective identification of cyclones and their circulation intensity, and climatology. *Wea. Forecasting,* **12,** 591–608.
Streten, N. A., and A. J. Troup, 1973: A synoptic climatology of satellite observed cloud vortices over the Southern Hemisphere. *Quart. J. Roy. Meteor. Soc.,* **99,** 56–72.
Taljaard, J. J., 1967: Development, distribution and movement of cyclones and anticyclones in the Southern Hemisphere during the IGY. *J. Appl. Meteor.,* **6,** 973–987.
Taylor, K. E., 1986: An analysis of biases in traditional cyclone frequency maps. *Mon. Wea. Rev.,* **114,** 1481–1490.
Trenberth, K. E., 1991: Storm tracks in the Southern Hemisphere. *J. Atmos. Sci.,* **48,** 2159–2178.
Wallace, J. M., G.-H. Lim, and M. L. Blackmon, 1988: Relationship between cyclone tracks, anticyclone tracks and baroclinic waveguides. *J. Atmos. Sci.,* **45,** 439–462.
Walsh, K., and I. G. Watterson, 1997: Tropical cyclone-like vortices in a limited area model: Comparison with observed climatology. *J. Climate,* **10,** 2240–2259.
Watterson, I. G., 1998: An analysis of the global water cycle of present and doubled CO_2 climates simulated by the CSIRO general circulation model. *J. Geophys. Res.,* **103,** 23 113–23 129
——, M. R. Dix, H. B. Gordon, and J. L. McGregor, 1995: The CSIRO nine-level atmospheric general circulation model and its equilibrium present and doubled CO_2 climates. *Aust. Meteor. Mag.,* **44,** 111–125.
——, S. P. O'Farrell, and M. R. Dix, 1997: Energy and water transport in climates simulated by a general circulation model that includes dynamic sea ice. *J. Geophys. Res.,* **102,** 11 027–11 037.
Whittaker, L. M., and L. H. Horn, 1984: Northern Hemisphere extratropical cyclone activity for four mid-season months. *J. Climatol.,* **4,** 297–310.
Zhang, Y., and W.-C. Wang, 1997: Model-simulated northern winter cyclone and anticyclone activity under a greenhouse warming scenario. *J. Climate,* **10,** 1616–1634.
Zishka, K. M., and P. J. Smith, 1980: The climatology of cyclones and anticyclones over North America and surrounding ocean environs for January and July, 1950–77. *Mon. Wea. Rev.,* **108,** 387–401.